

Effective models and predictability of chaotic multiscale systems via machine learning

Francesco Borra,^{1,*} Angelo Vulpiani,¹ and Massimo Cencini^{2,†}

¹*Dipartimento di Fisica, Università “Sapienza” Piazzale A. Moro 5, I-00185 Rome, Italy*

²*Istituto dei Sistemi Complessi, CNR, via dei Taurini 19, I-00185 Rome, Italy*

We scrutinize the use of machine learning, based on reservoir computing, to build data-driven effective models of multiscale chaotic systems. We show that, for a wide scale separation, machine learning generates effective models akin to those obtained using multiscale asymptotic techniques and, remarkably, remains effective in predictability also when the scale separation is reduced. We also show that predictability can be improved by hybridizing the reservoir with an imperfect model.

I. INTRODUCTION

Machine learning techniques are impacting science at an impressive pace from robotics [1] to genetics [2], medicine [3], and physics [4]. In physics, reservoir computing [5, 6], based on echo-state neural networks [7–9], is gathering much attention for model-free, data-driven predictions of chaotic evolutions [10–14]. Here, we scrutinize the use of reservoir computing to build effective models for predicting the slow degrees of freedom of multiscale chaotic systems. We also consider hybrid reservoirs, blending data with predictions based on an imperfect model [15] (see also [16]).

Multiscale chaotic systems represent a challenge to both theory and applications. For instance, turbulence can easily span over 4/6 decades in temporal/spatial scales [17], while climate time scales range from hours of atmosphere variability to thousands years of deep ocean [18, 19]. These huge ranges of scales stymie direct numerical approaches making modeling of fast degrees of freedom mandatory, being slow ones usually the most interesting to predict. In principle, the latter are easier to predict: the maximal Lyapunov exponent (of the order of the inverse of the fastest time scale) controls the early dynamics of very small perturbations appertaining to the fast degrees of freedom that saturate with time, letting the perturbations on the slow degrees of freedom to grow at a slower rate controlled by the typically weaker nonlinear instabilities [20–22]. However, owing to nonlinearity, fast degrees of freedom depend on, and in turn, impact on the slower ones. Consequently, improper modeling the former severely hampers the predictability of the latter [23].

We focus here on a simplified setting with only two time scales, i.e. on systems of the form:

$$\dot{\mathbf{X}} = \tau_s^{-1} \mathbf{F}_s(\mathbf{X}, \mathbf{x}), \quad \dot{\mathbf{x}} = \tau_f^{-1} \mathbf{F}_f(\mathbf{x}, \mathbf{X}), \quad (1)$$

where \mathbf{X} and \mathbf{x} represent the slow and fast degrees of freedom, respectively. The time scale separation between them is controlled by $c = \tau_s / \tau_f$. The goal is to build an effective model for the slow variables, $\dot{\mathbf{X}} = \mathbf{F}_{\text{eff}}(\mathbf{X})$, to

predict their evolution. When the fast variables are much faster than the slow ones ($c \gg 1$), multiscale techniques [24, 25] allow to build effective models. Aside from such limit, systematic methods for deriving effective models are typically unavailable.

In this article, we show that reservoir computers trained on time series of the slow degrees of freedom can be optimized to build effective models able to predict the slow dynamics. Provided the reservoir dimensionality is high enough, the method works both when the scale separation is large, basically recovering standard multiscale models, and when it not so large. We also show even an imperfect knowledge of the slow dynamics can be used to improve predictability, also for smaller reservoirs.

The material is organized as follows. In Sec. II we present the reservoir computing approach for predicting chaotic systems, moreover we provide the basics of its implementation also considering the case in which an imperfect model is available (hybrid implementation). In Sec. III we introduce the multiscale model we studied and show the main results. Section IV is devoted to discussions and perspectives. In Appendix A we give further details on implementation, including the choice of hyperparameters. Appendix B presents the adiabatic approximation for the multiscale system here considered. In Appendix C we discuss and compare different hybrid schemes.

II. RESERVOIR COMPUTING FOR CHAOTIC SYSTEMS AND ITS IMPLEMENTATION

Reservoir computing [5, 6] is a brain inspired approach based on a recurrent neural network (RNN), the reservoir (R) – i.e. an auxiliary high dimensional nonlinear dynamical system naturally suited to deal with time sequences –, (usually) linearly coupled to a time dependent lower dimensional input (I), to produce an output (O). To make O optimized for approximating some desired dynamical observable, the network must be trained. Reservoir computing implementation avoids backpropagation [26] by only training the output layer, while R-to-R and I-to-R connections are quenched random variables. Remarkably, the reservoir computing approach allows for fast hardware implementations with a variety of nonlinear systems [27, 28]. Choosing the output as a linear pro-

* Corresponding author; francesco.borra@uniroma1.it

† Corresponding author; massimo.cencini@cnr.it

jection of functions of the R-state, the optimization can be rapidly achieved via linear regression. The method works provided R-to-R connections are designed to force the R-state to only depend on the recent past history of the input signal, fading the memory of the initial state.

A. Predicting chaotic systems with reservoir computing

When considering a chaotic dynamical system with state $\mathbf{s}(t) = (\mathbf{X}(t), \mathbf{x}(t))$, with reference to Eq. (1), the input signal $\mathbf{u}(t) \in \mathbb{R}^{D_I}$ is typically a subset of the state observables, $\mathbf{u}(t) = \mathbf{h}(\mathbf{s}(t))$, for instance in the following we consider functions of the slow variables, \mathbf{X} , only. When the dimensionality, D_R , of the reservoir is large enough and the R-to-R connections are suitable chosen, its state, $\mathbf{r}(t) \in \mathbb{R}^{D_R}$, becomes a representation – an echo – of the input state $\mathbf{s}(t)$ [6, 9, 12], via a mechanism alike to generalized synchronization [12, 29]. In this configuration, dubbed open loop [30] (Fig. 1a), the RNN is driven by the input and, loosely speaking, synchronizes with it. When this is achieved, the output, $\mathbf{v}(t) \in \mathbb{R}^{D_O}$ can be trained (optimized) to fit a desired function of $\mathbf{s}(t)$, for instance, to predict the next outcome of the observable, i.e. $\mathbf{v}(t + \Delta t) = \mathbf{u}(t + \Delta t)$. After training, we can close the loop by feeding the output as a new input to R (Fig. 1b), thus obtaining an effective model for predicting the time sequence. For the closed loop mode to constitute an effective (neural) model of the dynamics of interest, we ask the network to work for arbitrary initial conditions, i.e. not only right after the training: a property dubbed *reusability* in [12]. For this purpose, when starting from a random reservoir state, a short synchronization period in open loop is needed before closing the loop. The method to work requires some stability property which cannot, in general, be granted in the closed loop configuration [30].

B. Implementation

Reservoir neurons can be implemented in different ways [5], here we use echo state neural network [9], mostly following [10–12]. Here, we assume $D_R \gg D_I = D_O$ and the input to be sampled at discrete time intervals Δt . Both assumptions are not restrictive, for instance in the hybrid implementation below we will use $D_O \neq D_I$ and the extension to continuous time is straightforward [5]. The reservoir is built via a sparse (low degree, d), random $D_R \times D_R$ connectivity matrix \mathbb{W}_R , with uniformly distributed entries in $[-1:1]$, scaled to have a specific spectral radius ρ – the largest eigenvalue. The request $\rho < 1$ is sufficient, though not strictly necessary [31], to ensure the echo state property [7, 8] in open loop, namely the synchronization of $\mathbf{r}(t)$ with $\mathbf{s}(t)$. We distinguish training and prediction. Training is done in open loop mode using an input trajectory $\mathbf{u}(t)$ with $t \in [-T_s : T_t]$ discretized

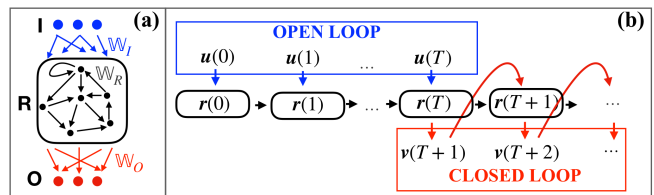


FIG. 1. (Color online) Sketch of reservoir computing: (a) the components and their connections; (b) the two modes of operation: open loop for synchronizing the reservoir to the input and for training, closed loop for prediction.

in steps of size Δt . T_s defines the length of initial transient to let the $\mathbf{r}(t)$, randomly initialized at $t = -T_s$, to synchronize with the system dynamics. While T_t is the training input sequence length. After being scaled to be zero mean and unit standard deviation, the input is linearly coupled to the reservoir nodes via a $D_R \times D_I$ matrix \mathbb{W}_I , with random entries uniform in $[-\sigma : \sigma]$. In open loop $\mathbf{r}(t)$ evolves as

$$\mathbf{r}(t + \Delta t) = \tanh[\mathbb{W}_R \mathbf{r}(t) + \mathbb{W}_I \mathbf{u}(t)], \quad (2)$$

where \tanh is applied element wise, and can be replaced with other nonlinearities. The output is computed as $\mathbf{v}(t + \Delta t) = \mathbb{W}_O \mathbf{r}^*(t + \Delta t)$ with the $D_R \times D_O$ matrix \mathbb{W}_O obtained via linear regression by imposing $\mathbb{W}_O = \arg \min_{\mathbb{W}} \{ \sum_{0 \leq t \leq T_t} \|\mathbf{v}(t) - \mathbf{u}(t)\|^2 + \alpha \text{Tr}[\mathbb{W}\mathbb{W}^T] \}$, to ensure the output to be the best predictor of the next input observable. The term proportional to α is a regularization, while \mathbf{r}^* is a function of the reservoir state. Here, we take $r_i^*(t) = r_i(t)$ if i is odd and $r_i^*(t) = r_i^2(t)$ otherwise [32]. Once \mathbb{W}_O is determined, we switch to prediction mode. Given a short sequence of measurements, in open loop, we can synchronize the reservoir with the dynamics (2), and then close the loop letting $\mathbf{u}(t) \leftarrow \mathbf{v}(t) = \mathbb{W}_O \mathbf{r}^*(t)$ in Eq. (2). This way Eq. (2) becomes a fully data driven effective model for the time signal to be predicted. The resulting model, and thus its performances, will implicitly depend on the hyperparameters (d , ρ and σ) defining the RNN structure and the I-to-R connections, and on the length of the training trajectory, their choice is discussed in Appendix A, where further details on the implementation can be found.

C. Hybrid implementation

So far we assumed no prior knowledge of the dynamical system that generated the input. If we have an imperfect model for approximately predicting the next outcome of the observables $\mathbf{u}(t)$, we can include such information in a hybrid scheme by slightly changing the input and/or output scheme to exploit this extra knowledge [15, 16]. The idea of blending machine learning algorithms with physics informed model is quite general and it has been exploited also with methods different from reservoir computing, see e.g. [33–35].

Let $\hat{\varphi}[\mathbf{u}(t)] = \hat{\mathbf{u}}(t + \Delta t)$ be the estimated next outcome of the observable $\mathbf{u}(t)$ according to our imperfect model.

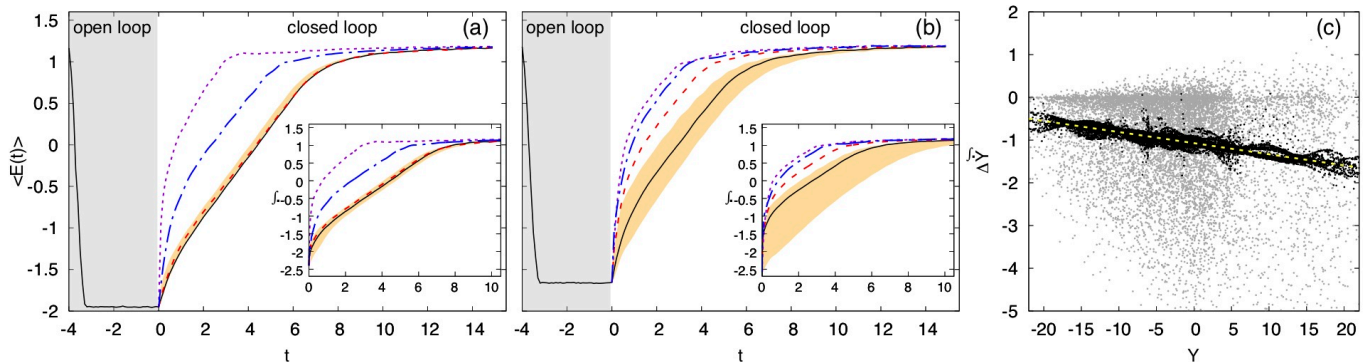


FIG. 2. (Color online) Prediction error growth (a-b) and network effective model (c), for a single realization of a network of $D_R=500$ neurons. (a) Average (over 10^4 initial conditions) $(\log_{10})\langle E(t) \rangle$ vs time during synchronization (open loop, gray region) and prediction (closed loop) for $c=10$ and $\Delta t=0.1$: the yellow shaded area circumscribes the twin and random twin model predictions (see text); reservoir computer prediction (solid, black curve) compared with that of the truncated model (purple, dotted curve), of the model fast variables replaced by their average (blue, dash dotted curve) and model (5) (red, dashed curve). The inset shows the same (closed loop only) for $\Delta t=0.01$. (b) Same as (a) for $c=3$. (c) Residual derivatives (6) vs Y for $c=10$ and $\Delta t=0.01$, computed with the network (black dots), the multiscale model (5) (yellow, dashed line), and the full dynamics (gray dots). For details on hyperparameters see Appendix A 6.

The idea is to supply such information in the input by replacing $\mathbf{u}(t)$ with the column vector $(\mathbf{u}(t), \varphi[\mathbf{u}(t)])^T$, thus doubling the dimensionality of the input matrix. For the output we proceed as before. The whole scheme is thus as the above one with the only difference that \mathbb{W}_O is now a $D_R \times D_I/2$. The switch to the prediction mode is then obtained using as input in Eq. (2) $(\mathbb{W}_O \mathbf{r}^*(t), \varphi[\mathbb{W}_O \mathbf{r}^*(t)])^T$. It is worth noticing that other hybrid schemes are possible, e.g. in Ref. [15] the output was in the form $\mathbf{v}(t+\Delta t) = \mathbb{W}_O(\mathbf{r}^*(t), \varphi[\mathbf{u}(t)])^T$, i.e. is a combination of the prediction based on the network and on the physical model. In Appendix C we comment further on our choice, and we compare it with the scheme proposed in Ref. [15].

III. RESULTS FOR A TWO TIME SCALES SYSTEM

We now consider the model introduced in [36] as a caricature for the interaction of the (fast) atmosphere and the (slow) ocean. It consists of two Lorenz systems coupled as follows:

$$\begin{cases} \dot{X} = a(Y - X) \\ \dot{Y} = R_s X - ZX - Y - \epsilon_s xy \\ \dot{Z} = XY - bZ \end{cases} \quad (3)$$

$$\begin{cases} \dot{x} = ca(y - x) \\ \dot{y} = c(R_f x - zx - y) + \epsilon_f Yx \\ \dot{z} = c(xy - bz), \end{cases} \quad (4)$$

where (3) and (4) describe the evolution of the slow and fast variables, respectively. We fix the parameters as in [36]: $a = 10$, $b = 8/3$, $R_s = 28$, $R_f = 45$, $\epsilon_s = 10^{-2}$ and $\epsilon_f = 10$, while for the time scale separation parameter, c , we use $c = 10$ (as in [36]) and $c = 3$. The former corresponds to a scale separation such that the adiabatic

approximation already provides good results (see below). Moreover, for $c=10$, the error growth on the slow variables is characterized by two exponential regimes [36]: the former with rate given by the Lyapunov exponent of the full system $\lambda_f \approx 11.5$, and the latter by $\lambda_s \approx 0.85$, controlled by the fast and slow instabilities, respectively. This decomposition can be made more rigorous as shown in [37] for a closely related model.

We test the reservoir computing approach inputting the slow variables, i.e. $\mathbf{u}(t) = (X(t), Y(t), Z(t))$. In open loop, we let the reservoir to synchronize with the input, subsequently we perform the training and optimize \mathbb{W}_O as explained earlier. Then, to test the prediction performance we consider 10^4 initial conditions, for each of which, we feed the slow variables to the network in open loop and record, from $t = -T_s$ to $t = 0$, the one step $(\log_{10})\text{error } E(t) = \log_{10} \|\mathbf{v}(t) - \mathbf{u}(t)\|$, $\mathbf{v}(t)$ being the one-step network forecast (output). The average $(\log_{10})\langle E(t) \rangle$ decreases linearly (a visual proof of the echo state property) and then reaches a plateau (see grey regions in Fig. 2a-b)- the synchronization error E_S - which can be interpreted as the average smallest (\log_{10}) error on the initial condition and the one step error prediction.

At the end of the open loop, after synchronization, we switch to the prediction (closed loop) configuration and compute the (\log_{10}) error growth between the predicted, by the network, and reference evolution. Moreover, we take the output variables at the end of the open loop and use them to initialize other models to be compared with the network, data-driven model. First, we consider the perfect model with an error on the initial condition, i.e Eqs. (3) with the slow variables set equal to the network obtained values at $t = 0$, i.e. at the end of the open loop. By construction, the network does not forecast the fast variables, which are thus initialized either using their exact values from the reference trajectory (twin

model), which is quite ‘unfair’, or random values (random twin) from the stationary measure on the fast attractor with fixed slow variables. Then we consider increasingly refined effective models for the slow degrees of freedom only: a “truncated” model, $\dot{\mathbf{X}} = \mathbf{F}_T(\mathbf{X})$, obtained from Eqs. (3) by setting $\epsilon_s = 0$, a model in which we replace the fast variables in Eqs. (3) with their global average or by their average with fixed slow variables – adiabatic approximation – which amounts to replacing $\epsilon_s xy$ in the equation for \dot{Y} with (see Appendix B for details on the derivation):

$$\epsilon_s \langle xy \rangle_{\mathbf{X}} = (1.07 + 0.26Y/c) \Theta(1.07 + 0.26Y/c), \quad (5)$$

being Θ the Heaviside step function.

In Fig. 2a and b we show the results of these comparisons for $c = 10$ and 3, respectively and sampling time $\Delta t = 0.1$ ($\Delta t = 0.01$ in the insets). When $c = 10$ and $\Delta t = 0.1$ (Fig. 2a), the network prediction is comparable to that of model (5) and of the twin model. Remarkably, it even slightly outperforms the latter. A fact we understand as follows: by omitting fast components it does not add fast decorrelating fluctuations to those intrinsic to the reference, thus reducing effective noise. Notice that the zero error on fast components of the twin model is rapidly pushed to its saturation value by the error on the slow variables. The sampling time $\Delta t = 0.1$ is likely playing an important role during learning by acting as a low passing filter. Indeed the comparison with twin model slightly deteriorates for $\Delta t = 0.01$ (see Fig. 2a inset). For $c = 3$, the poor scale separation spoils the effectiveness of model (5), see Fig. 2b. Moreover, discarded variables are not fast enough to average themselves out, making the learning task harder. Nevertheless, the network remains predictive.

A. Which effective model the network has built?

We now focus on the case $c = 10$ and $\Delta t = 0.01$, for which we can gain some insights into how the network works by comparing it to model (5). The sampling time is indeed small enough for time differences to approximate derivatives. In Fig. 2c we demonstrate that the network generates an effective model akin to the adiabatic one (5), by showing a surrogate of the residual time derivative of Y , i.e. by removing the truncated model derivative, as a function of Y :

$$\Delta \tilde{Y} = \frac{Y(t + \Delta t) - Y(t)}{\Delta t} - \frac{Y_T(t + \Delta t) - Y(t)}{\Delta t}, \quad (6)$$

this is a proxy of how the network has modeled the term $-\epsilon_s xy$ in Eq. (3). The underlying idea is as follows. We let the network evolve in closed loop, at time t it takes as input the forecasted slow variables $\mathbf{v}(t) = (\hat{X}(t), \hat{Y}(t), \hat{Z}(t))$ and outputs the next step forecast $\mathbf{v}(t + \Delta t) = (\hat{X}(t + \Delta t), \hat{Y}(t + \Delta t), \hat{Z}(t + \Delta t))$. We then use $\mathbf{v}(t)$ as input to the truncated model, and evolve it for

a time step Δt to obtain $(X_T(t + \Delta t), Y_T(t + \Delta t), Z_T(t + \Delta t))$. Equation (6) is then used to infer how the network models the coupling with the fast variables. Evolving by one time step $\mathbf{v}(t)$ using Eq. (5) and then again employing (6) we, obviously, obtain the line $-1.07 - 0.26Y$ (dashed in Fig. 2c). The network residual derivative (black dots in Fig. 2c) forms a narrow stripe around that line, meaning that the network, for wide scale separation, performs a conditional average which for $c = 10$ is equivalent to the adiabatic approximation (5). For comparison, we also show the residual derivative (6) for the full model (3-4) (gray dots), which displays large/fast oscillations that are indeed best fitted by (5). For $c = 3$, while the adiabatic approximation is too rough, remarkably the network still performs well even though is more difficult to identify the model it has built, which will depend on the whole set of slow variables (see discussion in App. B).

B. Predictability time and hybrid scheme

So far we focused on the predictability of a quite large network ($D_R = 500$ as compared to the low dimensionality of Eqs. (3-4)). How does the network performances depend on the reservoir size D_R ?

In Fig. 3 we show the D_R -dependence of the average (over reservoir realizations and initial conditions) predictability time, T_p , defined as the first time such that the error between the network predicted and reference trajectory reaches the threshold value $0.4(\|\mathbf{X}\|^2)^{1/2}$. For

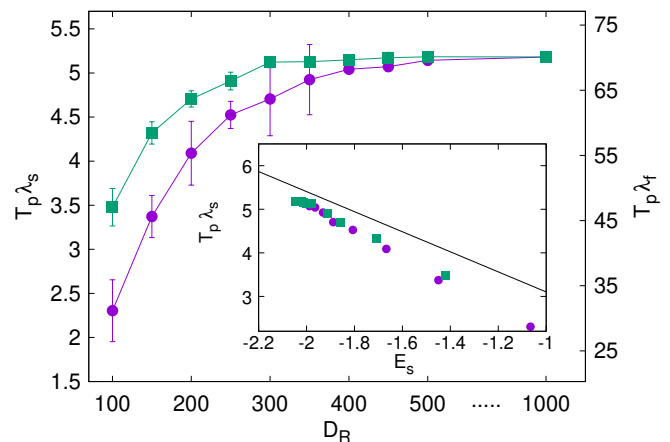


FIG. 3. (Color online) Average predictability time, T_p normalized with the slow finite size Lyapunov exponent λ_s (left scale) and with the (fast) maximal Lyapunov exponent λ_f (right scale), versus reservoir size D_R (hyperparameters for the hybrid implementation are the same of the reservoir only approach which are discussed in App. A 6) for reservoir only (purple circles) and hybrid scheme (green squares), system parameters $c = 10$ and $\Delta t = 0.1$. Error bars denote statistical standard deviation over 20 independent network realizations, each sampling 10^3 initial conditions. Inset: $T_p \lambda_s$ vs synchronization average $\langle E_S \rangle$. The slope of the black line is -1 corresponding to the slow perturbation growth rate λ_s .

$D_R \gtrsim 450$, the predictability time saturates while for smaller reservoirs it can be about threefold smaller and, in addition, with large fluctuations mainly due to unsuccessful predictions, i.e. instances in which the network is unable to properly model the dynamics (see Fig 4). Remarkably, implementing the hybrid scheme even with a poorly performing predictor such as the truncated model, the forecasting ability of the network improves considerably (as also shown in Fig. 3): saturation is reached earlier $D_R \gtrsim 300$ and, for smaller reservoirs, the predictability time of the hybrid scheme is longer. Moreover, the hybrid scheme is less prone to failures even for small D_R , hence fluctuations are smaller (see Fig. 4). Note that the chosen hybrid design ensures that the improvement is only due to reservoir capability of building a better effective model, reducing the average synchronization (\log_{10})error $\langle E_S \rangle$ (see the insets of Fig. 3 and 4, and the discussion in App. C) and thus the error on the initial condition of the slow variables. Indeed, in the inset of Fig. 3 we also show the slope predicted on the basis of the slow perturbation growth rate, λ_s [36].

Summarizing, the difference between hybrid and reservoir only approach disappears at increasing D_R as the same plateau values for both synchronization error and predictability time are reached. In other terms if the reservoir is large enough adding the extra information from the imperfect model does not improve the model produced by the network. Or, cast in a positive message, using a physically informed model allows for reducing the size of the reservoir to achieve a reasonable predictability and thus effective model of the dynamics.

We remark that in Fig. 3 the predictability time T_p was made nondimensional either using the growth rate of the slow dynamics λ_s (left scale of Fig. 3), or using the Lyapunov exponent of the full system λ_f (right scale) that is dominated by the fast dynamics. For large networks the predictability time is as large as 5 (finite size) Lyapunov times, which corresponds to about 70 Lyapunov times with respect to the full dynamics. This remarkable long predictability with respect to the fastest time scale is typical of multiscale systems, where the maximal Lyapunov exponent does not say much for the predictability of the slow degrees of freedom [20–22].

Figures 2a-b and 3(inset) (see also the inset of Fig. 4), show that it is hard reaching synchronization error below 10^{-2} . Even when this happens it does not improve the predictability, as the error quickly (even faster than the Lyapunov time) raises to that value. Indeed, such an error threshold corresponds to the crossover scale between the fast- and slow-controlled regime of the perturbation growth (see Fig. 2 in Ref. [36]). In other terms, pushing the error below this value requires the reservoir to (partially) reconstruct also the fast component dynamics.

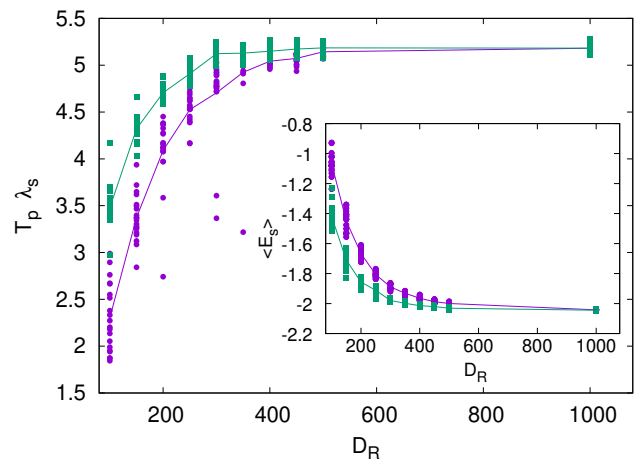


FIG. 4. (Color online) Nondimensional predictability time $T_p \lambda_s$ of 20 network realizations (each averaged over 10^4 initial conditions), in reservoir only (purple circles) and hybrid scheme (green squares), as a function of the reservoir size D_R . The solid curves display the average over all realizations, already presented in Fig. 3. Notice that, in the reservoir only scheme, a number of outliers are present for $D_R \lesssim 400$, these correspond to “failed” networks that make poor medium term predictions or even fail to reproduce the climate. Remarkably, such failures are not observed in the hybrid scheme. Inset: $\langle E_S \rangle$, i.e. the average (over network realizations and 10^4 initial conditions for each realization) (\log_{10})error at the end of the open loop versus the reservoir size D_R for the reservoir only (purple curve) and the hybrid (green curve) scheme, respectively. Symbols display the synchronization error in each network realization. Notice that there are no realizations with strong departure from the average as observed in main panel for the predictability time: this shows that the predictability performance is not always linked to the synchronization error (see text for a further discussion). Data refer to the case $c = 10$ and $\Delta t = 0.1$. For hyperparameters see App. A 6.

C. The role of the synchronization error

In the previous section, we have used as a performance metrics the average predictability time, T_p , namely the average time it takes an error to reach a given tolerance $\Delta^* = 0.4 \langle \|\mathbf{X}\|^2 \rangle^{1/2}$ after the synchronization period. Clearly, being the system chaotic and interpreting the synchronization error as an error on the initial conditions one can naively think that reducing such error always enhances the predictability, and, consequently, that the smallness of such error can be used as another performance metrics for the network. In the following we show that this is only partially true.

Clearly to achieve long term predictability the smallness of the synchronization error is a necessary condition. Indeed the (\log)error at the end of open loop cycle, E_S , puts an upper limit to the predictability time as

$$T_p \lesssim \frac{1}{\lambda_s} [\log(\Delta^*) - E_S], \quad (7)$$

as confirmed by the solid line in the inset of Fig. 3. How-

ever, it is not otherwise very informative about the overall performance. The reason is that the value of E_S , which can also be seen as the average error on one step predictions, does not provide information on the structural stability of the dynamics. Indeed, for a variety of hyperparameters values, we have observed low E_S resulting in failed predictions: in other terms the model built by the network is not effective in forecasting and in reproducing the climate. In these cases the network was unable to generate a good effective model, as shown in Fig. 4 this typically happens for relatively small D_R in the reservoir only implementation.

In a less extreme scenario, the error E_S can be deceptively lower than the scale at which the dynamics has been properly learned. This latter case is relevant to the multiscale setting since, as outlined at the end of the previous section, fast variable reconstruction is necessary to push the initial error below a certain threshold. In some cases, we did observe the synchronization error falling below the typical value 10^{-2} but immediately jumping back to it, implying unstable fast scale reconstruction (for instance, see $c = 3$, $\Delta t = 0.01$ in Fig. 2b).

As a consequence of the two above observations, E_S is an unreliable metric for hyperparameters landscape exploration as well. We also remark that, even if fast scales were modeled with proper architecture and training time, and E_S could be pushed below the crossover with an actual boost in performance, such improvements would not dramatically increase the predictability time of the slow variables, since they are suppressed by the global (and greater, as dominated by the fast degrees of freedom) Lyapunov exponent. This situation as discussed above is typical of multiscale systems.

IV. CONCLUSIONS

We have shown that reservoir computing is a promising machine learning tool for building effective, data driven models for multiscale chaotic systems able to provide, in some cases, forecasting as good as those that can be obtained with a perfect model with error on the initial conditions. Moreover, the simplicity of the system allowed us to gain insights into the inner work of the reservoir computing approach that, at least for large scale separation, is building an effective model akin to that obtained by asymptotic multiscale techniques. Finally, the reservoir computing approach can be reinforced by blending it with an imperfect predictor, making it to perform well also with smaller reservoirs. While we have obtained these results with a relatively simple two time scale model, given the success of previous applications to spatially extended systems [11], we think the method should work also with more complex high dimensional multiscale systems. In the latter, it may be necessary to consider multi reservoir architectures [38] in parallel [11]. Moreover, reservoir computing can be used to directly predict unobserved degrees of freedom [39]. Using this scheme and the ideas de-

veloped in this work it would be interesting to explore the possibility to build novel subgrid schemes for turbulent flows [40, 41] (see also [16] for a very recent attempt in this direction based on reservoir computing with hybrid implementation), preliminary tests could be performed in shell models for turbulence for which physics only informed approaches have been only partially successful [42].

ACKNOWLEDGMENTS

We thanks L. Biferale for early interest in the project and useful discussions. AV and FB acknowledge MIUR-PRIN2017 “Coarse-grained description for non-equilibrium systems and transport phenomena” (CONEST). We acknowledge the CINECA award for the availability of high performance computing resources and support from the GPU-AI expert group in CINECA.

Appendix A: Details on the implementation

1. Intra-reservoir (R-to-R) connectivity matrix \mathbb{W}_R

The intra-reservoir connectivity matrix, \mathbb{W}_R , is generated by drawing each entry from the same distribution. Each element is the product of two random variables $\mathbb{W}_{ij} = a * b$: a being a real uniformly distributed random number in $[-1 : 1]$ and b taking values 1 or 0 with probability $P_d = d/D_R$ and $1 - P_d$, respectively. Consequently, each row has, on average, d non zero elements. Since $D_R \gg d$, the number of non null entries per row is essentially distributed according to a Poisson distribution. As a last step, the maximal eigenvalue, $\rho_{\max}(\mathbb{W})$ of the resulting matrix \mathbb{W} is computed and the matrix is rescaled element wise so that its new spectral radius matches the target value ρ , i.e.:

$$\mathbb{W}_R = \mathbb{W} \frac{\rho}{\rho_{\max}(\mathbb{W})}$$

2. Input-to-reservoir (I-to-R) connectivity matrix \mathbb{W}_I

The input to reservoir matrix \mathbb{W}_I is generated in such a way that each reservoir node is connected to a single input. For this purpose, for each row j , a single element n_j , uniformly chosen between 1 and the input dimension D_I , is different from zero. This means that the reservoir node j is only connected to the n_j^{th} input node. The connection strength is randomly chosen in $[-\sigma, \sigma]$ with uniform distribution.

3. Optimization of the output matrix \mathbb{W}_O

The output matrix \mathbb{W}_O is obtained via optimization. As explained in Sec. IIB, \mathbb{W}_O should be chosen so that the output $\mathbf{v}(t) = \mathbb{W}_O \mathbf{r}^*(t)$ is, on average, as similar as possible to the input signal $\mathbf{u}(t)$. Incidentally, we remark that the use of \mathbf{r}^* instead of simply \mathbf{r} is relevant to achieve accurate forecasting and is heuristically motivated by the need to add some nonlinearity in the network [7]. The particular choice we adopted, $r_i^* = r_i$ or r_i^2 for i odd or even, respectively was suggested in [10, 12] in view of the symmetries of the Lorenz model.

As for the optimization of \mathbb{W}_O , we require that it should minimize the cost function

$$\mathcal{L} = \frac{1}{T_t} \sum_{0 \leq t \leq T_t} \|\mathbb{W}_O \mathbf{r}^*(t) - \mathbf{u}(t)\|^2 + \alpha \text{tr}[\mathbb{W}_O \mathbb{W}_O^T], \quad (\text{A1})$$

where T denotes the transpose and T_t is the length of the training input, whose choice is discussed below. We point out that the sum appearing in Eq. (A1) is a delicate quantity: we have observed that moderate errors compromise the final performance. For this reason, the Kahan summation has been employed in order to boost numerical accuracy. The solution of the minimization of Eq. (A1),

$$\mathbb{W}_O^{\text{opt}} \text{ so that } \left. \frac{d\mathcal{L}}{d\mathbb{W}_O^T} \right|_{\mathbb{W}_O^{\text{opt}}} = 0$$

is

$$\mathbb{W}_O^{\text{opt}} = \langle \mathbf{u} \otimes \mathbf{r}^{*T} \rangle (\alpha \mathbb{I}_{D_R} + \langle \mathbf{r}^* \otimes \mathbf{r}^{*T} \rangle)^{-1}$$

where $\langle \cdot \rangle$ denotes the empirical average $\frac{1}{T_t} \sum_t$, \otimes denotes the outer product and \mathbb{I}_{D_R} the $D_R \times D_R$ identity matrix. The addend proportional to α in Eq. (A1) is the Tikhonov term, which is a L^2 regularization on \mathbb{W}_O . The Tikhonov regularization improves the numerical stability of the inversion, which could be critical if the ratio between the largest and the smallest eigenvalues, ρ_{\max} and ρ_{\min} , is too large and the latter would behave as a (numerical) null eigenvalue [43], as it is the case for the dynamics we are studying. Here we have used $\alpha = 10^{-8.5}$ which empirically was found to lead to $\log_{10}(\rho_{\max}/\rho_{\min}) \approx 10$.

4. Synchronization time and length of the training input trajectory

All results presented in this article have been obtained using training trajectories of length $T_t = 500$. We remark that using values $100 \leq T_t \leq 1000$ one can hardly notice qualitative differences. At low training times, failures can be qualitative very diverse, ranging from tilted attractors to periodic orbits or spurious fixed points. The chosen values of T_t have been tested to be in the range that guarantees long term reconstruction of the attractor with

proper hyperparameters. As for the the synchronizing length, we have chosen $T_s = 4$. Such value is about four times larger than the time actually needed to achieve best possible synchronization indeed, as shown in the gray shaded areas of Figs. 2a-b, the error E saturates to E_S in about a time unit.

5. Numerical details

The whole code has been implemented in *python3*, with linear algebra performed via *numpy*. Numerical integration of the coupled Lorenz model were performed via a 4th order Runge Kutta scheme.

6. Fixing the hyperparameters

The architecture of a generic network is described by a number of parameters, often dubbed hyperparameters, e.g.: the number of layers, activation functions etc. While a proper design is always crucial, in the reservoir computing paradigm, this issue is especially critical due to the absence of global optimization via backpropagation. The reservoir-to-reservoir and input-to-reservoir connectivity matrices, as discussed above, are quenched stochastic variables, whose distribution depends on four hyperparameters:

$$\text{Net} \sim P(\sigma, \rho, d, D_R),$$

namely, the strength of the I-to-R connection matrix, σ , the spectral radius, ρ , and the degree, d , of the R-to-R connection matrix, and the reservoir size D_R . Once the distribution is chosen, there are two separate issues.

The first is that, for a given choice of (σ, ρ, d) , the network should be self-averaging if its size D_R is large enough. Indeed, we see from Fig. 4 that the variability between realizations decreases with D_R , as expected.

The second issue is the choice of the triple (σ, ρ, d) . In general, the existence of large and nearly flat (for any reasonable performance metrics) region of suitable hyperparameters implies the robustness of the method. As for the problem we have presented, such region exists, even though, in the case $\Delta t = 0.1$, $c = 10$, moderate fine tuning of the hyperparameters did improve the final result, allowing to even (moderately) outperform the fully informed twin model, as shown in Fig. 2a.

It is important to remark that the characteristics of the regions of suitable hyperparameters depend on the used metric. Here, we have focused on medium term predictability, i.e. we evaluate the error between forecasted and reference slow variables at a time (after synchronization) that is much larger than one step Δt but before error saturation (corresponding to trajectories completely uncorrelated). Requiring a too short time predictability, as discussed in Ref. [12], typically is not enough for reproducing long time statistical properties of the target

system (i.e. the so called climate), as the learned attractor may be unstable even if the dynamical equations are locally well approximated. If both short term predictability and climate reproduction are required, the suitable hyperparameter region typically shrinks. The metric we used typically led to both predictability and climate reproduction, at least for reservoir sizes large enough.

In order to fix the parameters, two techniques have been employed. The first is the standard search on a grid (for a representative example see Fig. 5): a lattice is generated in the space of parameters, then each node is evaluated according to some cost function metrics. If such function is regular enough, it should be possible to detect a suitable region of parameters. While this default method is sound, it may require to train many independent networks, even in poorly performing regions. Each network cannot be too small for two reasons: the first is that small networks suffer from higher inter realization fluctuations, the second is that we cannot exclude that optimal (σ, ρ, d) have a loose dependence on the reservoir size D_R . As further discussed below we found a mild dependence on the network degree d , provided it is not too large, thus in Fig.5 we focused on the dependence on ρ and σ .

The second technique is the no gradient optimization method known as particle swarming optimization (PSO) [44]. PSO consists in generating n (we used $n = 10$) tuples of candidate – the particles – parameters, say $\mathbf{p}_i = (\rho_i, \sigma_i, d_i)$ $i = 1, \dots, n$. At each step, each candidate is tested with a given metrics f . Here, we used the average (over 50 – 100 initial conditions) error on the slow variables after $t = 2, 4, 5$ (depending on the parameters) in the close loop configuration. Then, at each iteration k of the algorithm, each candidate is accelerated

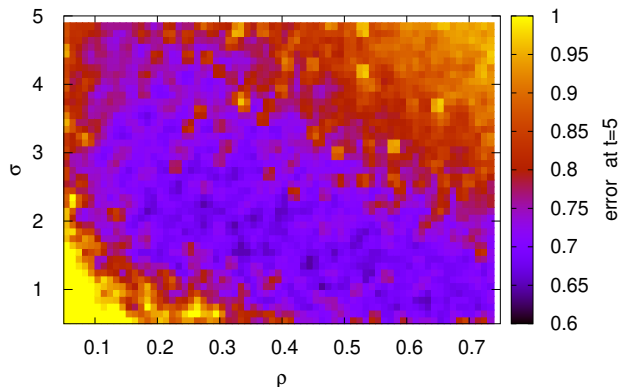


FIG. 5. (Color online) Performance grid for $c = 3$, $\Delta t = 0.1$, $N = 350$, $d = 5$. Colors code error between forecasted and reference trajectory at time $t = 5$ after closing the loop, which if the metrics here used $f = \|\mathbf{X}^{forecast}(t = 5) - \mathbf{X}^{true}(t = 5)\|$ (averaged over 100 points of the attractor) for a single realization of the network for a given value of parameters (ρ, σ) . To highlight the suitable parameter region, a cutoff on has been put at $f = 1$.

towards a stochastic mixture of its own best performing past position

$$\mathbf{p}_i^*(k) = \arg \min_{\mathbf{p}_i(s)} \{f(\mathbf{p}_i(s)) | s < k\}$$

and the overall best past performer

$$\mathbf{p}^*(k) = \arg \min_{\mathbf{p}_i^*(k)} \{f(\mathbf{p}_i^*(k)) | i = 1, \dots, n\}.$$

Particles are evolved with the following second order time discrete dynamics

$$\begin{aligned} \mathbf{p}_i(k+1) &= \mathbf{p}_i(k) + \mathbf{v}_i(k) \\ \mathbf{v}_i(k+1) &= w\mathbf{v}_i(k) + \phi_i^1(k) (\mathbf{p}_i^*(k) - \mathbf{p}_i(k)) \\ &\quad + \phi_i^2(k) (\mathbf{p}^*(k) - \mathbf{p}_i(k)) \end{aligned}$$

with $\phi_i^j(k) \in [0, 1]$ being random variables and $w \in [0, 1]$ representing a form of inertia, as implemented in the python library *pyswarms*. After a suitable amount of iterations, \mathbf{p}^* should be a valid candidate. The advantage of PSO is that, after a transient, most candidate evaluations (each of which require to initialize, train and test at least one network) should happen in the good regions. It is worth pointing out that, unless self-averaging is achieved thanks to large enough reservoir sizes, inter network variability adds noise to limited attractor sampling when evaluating f and, therefore, fluctuations may appear and trap the algorithm in suboptimal regions for some time. Moreover, the algorithm itself depends on some hyperparameters that may have to be optimized themselves by hand.

In our study, PSO has been mainly useful in fixing parameters in the $(\Delta t = 0.1, c = 10)$ case and to observe that d is the parameter which affects the performance the least. Some gridding (especially in ρ and σ) around the optimal solution is useful, in general, as a cross check and to highlight the robustness (or lack thereof) of the solution.

In Table I we summarize the hyperparameters used in our study.

	$\Delta t = 0.1$	$\Delta t = 0.01$
$c=3$	$d = 5$ $\sigma = 2$ $\rho = 0.35$	$d = 5$ $\sigma = 2.5$ $\rho = 0.25$
$c=10$	$d = 5$ $\sigma = 1.8$ $\rho = 0.34$	$d = 5$ $\sigma = 0.8$ $\rho = 0.68$

TABLE I. (Color online) Hyperparameters used in the simulations: Δt is the sampling time, c is the time scale separation of the multiscale scale Lorenz model Eq. (3-4), σ is the input-to-reservoir coupling strength, ρ is spectral radius of the reservoir-to-reservoir connectivity matrix and d its degree. For the hybrid implementation, discussed in Sec. II C and App. C we used the same hyperparameters.

Appendix B: Multiscale model for the two time scales coupled Lorenz systems

In this Appendix we show how Eq. (5) was derived. Following the notation of Eq. (1), we will denote with \mathbf{X} and \mathbf{x} the slow (X, Y, Z) and fast (x, z, y) variables, respectively. Our aim is to provide a model of the fast variables in Eq. (3) in terms of the slow ones. When the former are much faster than the latter, we can assume that \mathbf{x} equilibrates, i.e. distribute according to a stationary measure, for each value of the slow variables \mathbf{X} – adiabatic principle –, and we call the expected values with respect to such measure as $\langle \cdot \rangle_{\mathbf{X}}$. The adiabatic approach can work only for a wide scale separation ($c \gg 1$). In this limit, since only Y enters the dynamics of the fast variables, only the value of Y will matter in building the adiabatic approximation, i.e. $\langle \cdot \rangle_{\mathbf{X}} \equiv \langle \cdot \rangle_Y$. In general, for moderate scale separation, this is not the case and a “closure” of the fast variables depending on the whole set of slow variables would be required, a much harder task.

In order to model $\langle xy \rangle_{\mathbf{X}}$, we first impose stationarity i.e. $\langle \dot{\mathbf{x}} \rangle_{\mathbf{X}} = 0.$, which applied to the third line of (4) yields

$$\langle xy \rangle_{\mathbf{X}} = b \langle z \rangle_{\mathbf{X}}. \quad (\text{B1})$$

Inserting (B1) in the equation for Y in (3) we obtain $\dot{Y} = R_s X - Z X - Y - \epsilon_s b \langle z \rangle_{\mathbf{X}}$. Now we need to determine $\langle z \rangle_{\mathbf{X}}$. For this purpose, we notice that the equation for \dot{y} in (4) can be rewritten as

$$\dot{y} = c[Rx - zx - y] \quad \text{with} \quad R = R_f + \frac{\epsilon_f}{c} Y \quad (\text{B2})$$

Exploiting the adiabatic principle we assume Y (the slow variable) as fixed so that Eq. (4) with the second equation substituted with Eq. (B2) becomes the standard Lorenz model, a part from an inessential change of time scale.

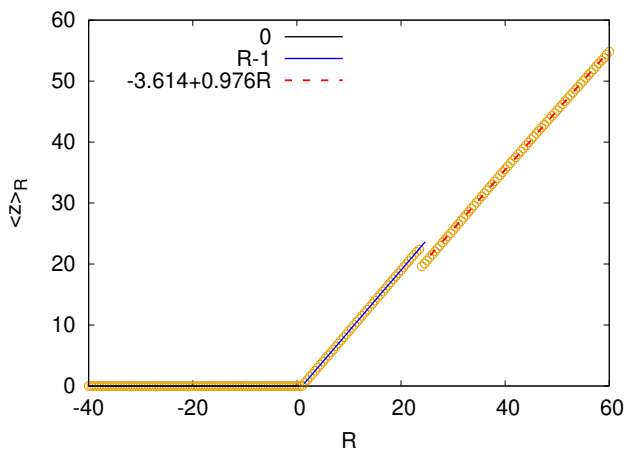


FIG. 6. (Color online) $\langle z \rangle_R$ vs R numerically computed in the standard Lorenz system (symbols). Notice that the curve is well approximated, in the range of interest, by the piecewise linear function (B3), see legend.

Thus, we can now evolve the standard Lorenz model and compute $\langle z \rangle_R$ (where R is just to remind the R dependence that will be reflected in a Y dependence via (B2)), which is shown in Fig. 6. As one can see $\langle z \rangle_R$ depends on R approximately as follows:

$$\langle z \rangle_R \approx \begin{cases} 0 & R < 1 \\ R - 1 & 1 \leq R \lesssim 24.74 \\ 0.976R - 3.614 & R \gtrsim 24.74 \end{cases} \quad (\text{B3})$$

We remind that $R_c = 24.74$ is the critical value at which the fixed point

$$z^* = (R - 1)\Theta(R - 1), \quad (\text{B4})$$

(where Θ is the Heaviside step function) loses its stability. Remarkably, $\langle z \rangle_R$ remain close to z^* also for $R > R_c$. The second expression in Eq. (B3), or equivalently Eq. (B4), yields

$$\langle xy \rangle_Y = b(R_f - 1 + (\epsilon_f/c)Y)\Theta(R_f - 1 + (\epsilon_f/c)Y). \quad (\text{B5})$$

Using the numerical values of the constants ($b = 8/3$, $R_f = 45$ and $\epsilon_f = 10$), the above expression provides the estimate $\langle xy \rangle_Y \approx (117.33 + 26.67Y/c)\Theta(117.33 + 26.67Y/c)$ while using the third expression of Eq. (B3) yields model (5) that we used to compare with the network, i.e.

$$\langle xy \rangle_Y = (107.5 + 26.04Y/c)\Theta((107.5 + 26.04Y/c)). \quad (\text{B6})$$

For $c = 10$, the latter expression is very close to the (numerically obtained) conditional average $\langle xy|Y \rangle$ (Fig. 7a), confirming that the scale separation is wide enough for the adiabatic approximation to work almost perfectly. We notice that for $c = 10$ the typical range of variation of Y is such that R mostly lies in the region of the third branch of (B3), explaining the validity of the approximation.

Conversely, for the case $c = 3$, as shown in Fig. 7b the approximation is much cruder and important deviations are present especially for large positive values of Y . Indeed, in general,

$$\langle xy \rangle_{\mathbf{X}} \neq \langle xy|\mathbf{X} \rangle$$

i.e. multiscale average obtained via the adiabatic principle and the conditional average are not equivalent since, in general, $\langle \dot{\mathbf{x}}|\mathbf{X} \rangle \neq 0$. In this case the values of all slow variables will matter in building a proper effective model, a hard task even for the simple Lorenz model here considered. However, as shown in Fig. 2b, even in this case the reservoir computing approach is quite performing even though it is not straightforward to decipher the model it was able to devise.

Appendix C: Discussion on various hybrid schemes implementations

The hybrid scheme discussed in Sec. II C allows for highlighting the properties of the reservoir, but it is just

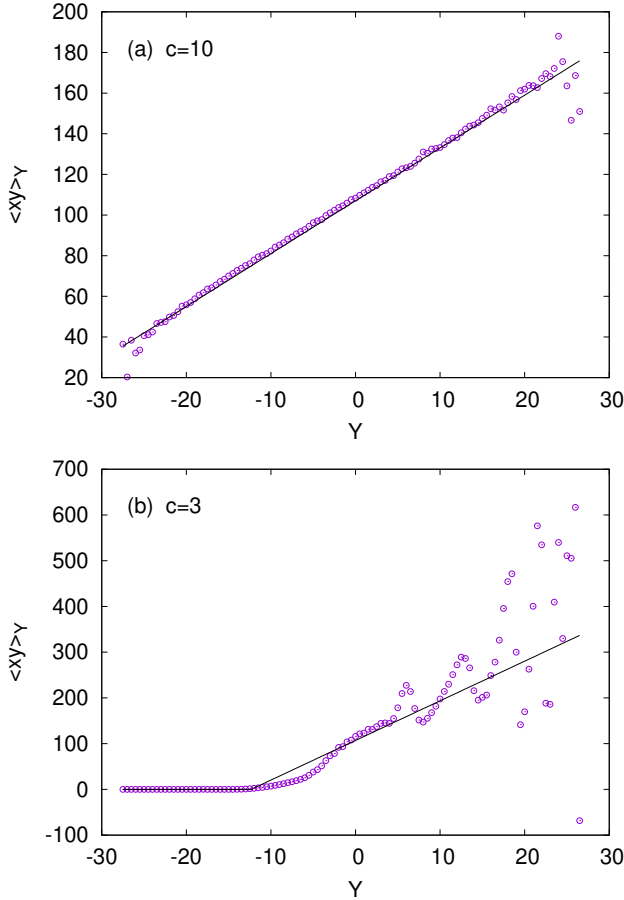


FIG. 7. (Color online) Numerically computed conditional averages (symbols) $\langle xy|Y \rangle$ for (a) $c = 10$ and (b) $c = 3$ and the corresponding multiscale (adiabatic) averages $\langle xy \rangle_Y$ given by Eq. (B6) (solid curve). For $c = 10$ the two curves overlap.

one possible choice. Here, we briefly discuss three general schemes.

Let us assume, for simplicity, that our dynamical system, with state variables $\mathbf{s} = (s_1, \dots, s_n)$, is described by the equation $\mathbf{s}(t+1) = \mathbf{f}(\mathbf{s}(t))$, which is unknown. Here, without loss of generality, we use discrete time dynamics and that we want to forecast the whole set of state variables, this is just for the sake of simplicity of the presentation. Provided we have an imperfect model, $\mathbf{s}(t+1) \approx \mathbf{f}_m(\mathbf{s}(t))$, for its evolution, we have basically three options for building a hybrid scheme.

A first possibility is to approximate via machine learning only the part of the signal that is not captured by the model $\mathbf{f}_m(\mathbf{s}(t))$. In other terms, one writes a forecast as

$$\hat{\mathbf{s}}(t+1) = \mathbf{f}_m(\mathbf{s}(t)) + \delta_n(\mathbf{s}(t)) \quad (\text{C1})$$

where the residual δ_n is given by the network, and can be learned from a set of input-output pairs $\{\mathbf{s}(t), \mathbf{s}(t+1) - \mathbf{f}_m(\mathbf{s}(t))\}_{t=-T}^0$ according to some supervised learning algorithm. In our framework, the hybrid network should be trained with the usual input but with target output

given by the difference between the true value of $\mathbf{s}(t+1)$ and the model forecast $\mathbf{f}_m(\mathbf{s}(t))$.

A second possibility is to add the available model prediction $\mathbf{f}_m(\mathbf{s}(t))$ to the input $\mathbf{s}(t)$, obtaining an augmented input $(\mathbf{s}(t), \mathbf{f}_m(\mathbf{s}(t)))$ for the network. In this case, the forecast reads as

$$\hat{\mathbf{s}}(t+1) = \mathbf{f}_n(\mathbf{s}(t), \mathbf{f}_m(\mathbf{s}(t))). \quad (\text{C2})$$

Clearly, if the model based prediction is very accurate, the network will try to approximate the identity function. The network should be trained with a set of input-outputs pairs $\{(\mathbf{s}(t), \mathbf{f}_m(\mathbf{s}(t))), \mathbf{s}(t+1)\}_{t=-T}^0$. This is the approach we have implemented in this article, in order to evaluate the performance of the reservoir.

A third possibility, which should be as least as good as the best option between the previous two (unless very poor design choices are made) mixes the above two by computing a residual with a model informed network, this is the approach, e.g., described in [15]. In this case the forecast is obtained as:

$$\hat{\mathbf{s}}(t+1) = \mathbb{A} \mathbf{f}_m(\mathbf{s}(t)) + \mathbb{B} \delta_n(\mathbf{s}(t), \mathbf{f}_m(\mathbf{s}(t))), \quad (\text{C3})$$

where the matrices \mathbb{A} and \mathbb{B} should be optimized, along with δ_n [15]. This last option is a special case of the second scheme, describing a residual multilayered neural network with a linear output layer.

For the sake of completeness, in Fig. 8 we show how this last architectures compares with the one we used in Figs. 3 and 4 in terms of predictability. It consists in taking the optimized linear combination of the predictions from the hybrid net and the imperfect model. Namely, one augment the \mathbf{r}^* array as $\tilde{\mathbf{r}}^* = (\mathbf{r}^*, \mathbf{f}_m)$ and then optimists \mathbb{W}_O to achieve $\mathbf{v}(t+1) = \hat{\mathbf{s}}(t+1) \approx \mathbb{W}_O \tilde{\mathbf{r}}^*(t)$. As one can see, the main effect is to slightly shift the

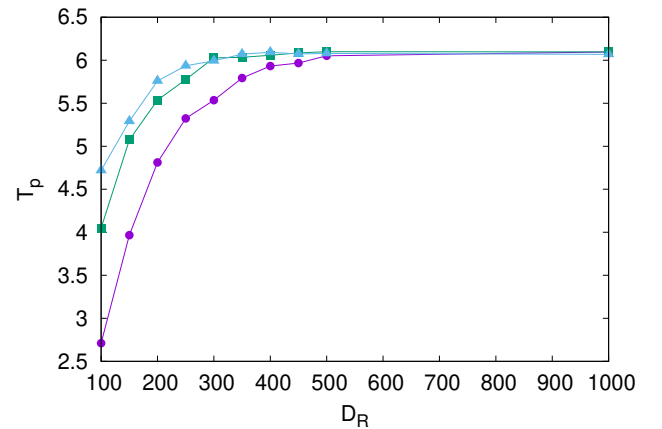


FIG. 8. (Color online) Average (over 10^4 initial conditions) predictability times are shown for reservoir only and two hybrid implementations ($\Delta t = 0.1$ and $c = 10$). The green line corresponds hybrid scheme (C2), blue lines to hybrid scheme (C3) and purple lines to reservoir only baseline.

predictability-vs-size curve leftward, meaning that optimal performance can be achieved with a slightly smaller

network. However, the improvement quickly disappears when the reservoir size increases.

-
- [1] B. D. Argall, S. Chernova, M. Veloso, and B. Browning, *Robot. Auton. Sys.* **57**, 469 (2009).
- [2] M. W. Libbrecht and W. S. Noble, *Nature Rev. Genet.* **16**, 321 (2015).
- [3] J. He, S. L. Baxter, J. Xu, J. Xu, X. Zhou, and K. Zhang, *Nature Med.* **25**, 30 (2019).
- [4] G. Carleo, I. Cirac, K. Cranmer, L. Daudet, M. Schuld, N. Tishby, L. Vogt-Maranto, and L. Zdeborová, *Rev. Mod. Phys.* **91**, 045002 (2019).
- [5] D. Verstraeten, B. Schrauwen, M. dHaene, and D. Stroobandt, *Neural Net.* **20**, 391 (2007).
- [6] B. Schrauwen, D. Verstraeten, and J. Van Campenhout, in *Proc. 15th Europ. Symp. Artif. Neural Netw.* (2007) pp. 471–482.
- [7] H. Jaeger, German Nat. Res. Center Infor. Tech. GMD Technical Report **148**, 13 (2001).
- [8] M. Lukoševičius and H. Jaeger, *Comp. Sci. Rev.* **3**, 127 (2009).
- [9] H. Jaeger and H. Haas, *Science* **304**, 78 (2004).
- [10] J. Pathak, Z. Lu, B. R. Hunt, M. Girvan, and E. Ott, *Chaos* **27**, 121102 (2017).
- [11] J. Pathak, B. Hunt, M. Girvan, Z. Lu, and E. Ott, *Phys. Rev. Lett.* **120**, 024102 (2018).
- [12] Z. Lu, B. R. Hunt, and E. Ott, *Chaos* **28**, 061104 (2018).
- [13] P. R. Vlachas, W. Byeon, Z. Y. Wan, T. P. Sapsis, and P. Koumoutsakos, *Proc. Royal Soc. A* **474**, 20170844 (2018).
- [14] K. Nakai and Y. Saiki, *Phys. Rev. E* **98**, 023111 (2018).
- [15] J. Pathak, A. Wikner, R. Fussell, S. Chandra, B. R. Hunt, M. Girvan, and E. Ott, *Chaos* **28**, 041101 (2018).
- [16] A. Wikner, J. Pathak, B. Hunt, M. Girvan, T. Arcomano, I. Szunyogh, A. Pomerance, and E. Ott, *Chaos* **30**, 053111 (2020).
- [17] Z. Warhaft, *Proc. Nat. Acad. Sci.* **99**, 2481 (2002).
- [18] J. P. Peixoto and A. H. Oort, *Physics of climate* (New York, NY (United States); American Institute of Physics, 1992).
- [19] J. Pedlosky, *Geophysical fluid dynamics* (Springer, 2013).
- [20] E. N. Lorenz, in *ECMWF Seminar Proceedings on Predictability*, Vol. 1 (ECMWF, Reading, UK, 1995).
- [21] E. Aurell, G. Boffetta, A. Crisanti, G. Paladin, and A. Vulpiani, *Phys. Rev. Lett.* **77**, 1262 (1996).
- [22] M. Cencini and A. Vulpiani, *J. Phys. A* **46**, 254019 (2013).
- [23] G. Boffetta, A. Celani, M. Cencini, G. Lacorata, and A. Vulpiani, *J. Phys. A* **33**, 1313 (2000).
- [24] J. A. Sanders, F. Verhulst, and J. Murdock, *Averaging methods in nonlinear dynamical systems*, Vol. 59 (Springer, 2007).
- [25] G. Pavliotis and A. Stuart, *Multiscale methods: averaging and homogenization* (Springer, 2008).
- [26] P. J. Werbos, *Proc. IEEE* **78**, 1550 (1990).
- [27] L. Larger, A. Baylón-Fuentes, R. Martinenghi, V. S. Udaltsov, Y. K. Chembo, and M. Jacquot, *Physical Review X* **7**, 011015 (2017).
- [28] G. Tanaka, T. Yamane, J. B. Héroux, R. Nakane, N. Kanazawa, S. Takeda, H. Numata, D. Nakano, and A. Hirose, *Neural Net.* **115**, 100 (2019).
- [29] A. Pikovsky, J. Kurths, and M. Rosenblum, *Synchronization: a universal concept in nonlinear sciences*, Vol. 12 (Cambridge university press, 2003).
- [30] A. Rivkind and O. Barak, *Phys. Rev. Lett.* **118**, 258101 (2017).
- [31] J. Jiang and Y.-C. Lai, *Phys. Rev. Res.* **1**, 033056 (2019).
- [32] In [10, 12] it is suggested that this choice respects the symmetries of the Lorenz system. In general, it is expected that reasonably nonlinear function of r_i should suffice [7].
- [33] M. Milano and P. Koumoutsakos, *J. Comput. Phys.* **182**, 1 (2002).
- [34] Z. Y. Wan, P. Vlachas, P. Koumoutsakos, and T. Sapsis, *PloS one* **13**, e0197704 (2018).
- [35] G. D. Weymouth and D. K. P. Yue, *J. Ship Res.* **57**, 1 (2013).
- [36] G. Boffetta, P. Giuliani, G. Paladin, and A. Vulpiani, *J. Atmos. Sci.* **55**, 3409 (1998).
- [37] M. Carlu, F. Ginelli, V. Lucarini, and A. Politi, *Nonlin. Proc. Geophys.* **26**, 73 (2019).
- [38] Z. Carmichael, H. Syed, and D. Kudithipudi, in *Proc. 7th Annual Neuro-inspired Comput. Elements Workshop* (2019) pp. 1–10.
- [39] Z. Lu, J. Pathak, B. Hunt, M. Girvan, R. Brouckett, and E. Ott, *Chaos* **27**, 041102 (2017).
- [40] C. Meneveau and J. Katz, *Annu. Rev. Fluid Mech.* **32**, 1 (2000).
- [41] P. Sagaut, *Large eddy simulation for incompressible flows: an introduction* (Springer, 2006).
- [42] L. Biferale, A. A. Mailybaev, and G. Parisi, *Phys. Rev. E* **95**, 043108 (2017).
- [43] Notice that if $T_i/\Delta t < D_R$ at least one eigenvalue is zero.
- [44] J. Kennedy and R. Eberhart, in *Proceedings of ICNN'95-International Conference on Neural Networks*, Vol. 4 (IEEE, 1995) pp. 1942–1948.